Eur. Phys. J. C (2022) 82:1135
https://doi.org/10.1140/epjc/s10052-022-11051-z

THE EUROPEAN PHYSICAL JOURNAL C

Regular Article - Theoretical Physics

# The CDF $W$-mass, muon $g-2$, and dark matter in a $U(1)_{L_\mu - L_\tau}$ model with vector-like leptons

**Quan Zhou, Xiao-Fang Han, Lei Wang**[a]

Department of Physics, Yantai University, Yantai 264005, People's Republic of China

Received: 3 May 2022 / Accepted: 18 November 2022 / Published online: 15 December 2022


**Abstract** We study the CDF $W$-mass, muon $g-2$, and dark matter observables in a local $U(1)_{L_\mu - L_\tau}$ model in which the new particles include three vector-like leptons ($E_1,\ E_2,\ N$), a new gauge boson $Z'$, a scalar $S$ (breaking $U(1)_{L_\mu - L_\tau}$), a scalar dark matter $X_I$ and its partner $X_R$. We find that the CDF $W$-mass disfavors $m_{E_1} = m_{E_2} = m_N$ or $s_L = s_R = 0$ where $s_{L(R)}$ is mixing parameter of left (right)-handed fields of vector-like leptons. A large mass splitting between $E_1$ and $E_2$ is favored when the differences between $s_L$ and $s_R$ becomes small. The muon $g-2$ anomaly can be simultaneously explained for appropriate difference between $m_{E_1}$ ($s_L$) and $m_{E_2}$ ($s_R$), and some regions are excluded by the diphoton signal data of the 125 GeV Higgs. Combined with the CDF $W$-mass, muon $g-2$ anomaly and other relevant constraints, the correct dark matter relic density is mainly obtained in two different scenarios: (i) $X_I X_I \to Z'Z',\ SS$ for $m_{Z'}(m_S) < m_{X_I}$ and (ii) the co-annihilation processes for $min(m_{E_1}, m_{E_2}, m_N, m_{X_R})$ close to $m_{X_I}$. Finally, we use the direct searches for $2\ell + E_T^{miss}$ event at the LHC to constrain the model, and show the allowed mass ranges of the vector-like leptons and dark matter.

## 1 Introduction

Recently, the CDF collaboration reported their new measurement of the $W$-boson mass [1]

$$m_W = 80.4335 \pm 0.0094 \text{ GeV}, \tag{1}$$

which approximately has $7\sigma$ deviation from the Standard Model (SM) value, $80.357 \pm 0.006$ GeV [2]. This CDF value is in significant tension with the other experiment measurements including the most precise one reported by the ATLAS collaboration, $m_W = 80.370 \pm 0.019$ GeV [3]. Here we take the CDF result seriously and discuss implication of the $W$-mass shift on new physics models. Besides, the FNAL experiment measurement of the muon anomalous magnetic moment (muon $g-2$) [4], when combined with the result of the BNL experiment [5,6], has an approximate $4.2\sigma$ discrepancy from the SM prediction [7–9],

$$\Delta a_\mu = a_\mu^{exp} - a_\mu^{SM} = (25.1 \pm 5.9) \times 10^{-10}. \tag{2}$$

The two anomalies both call for new physics beyond SM. There have been many works explaining the CDF $W$-mass [10–79].

In this paper, we study the CDF $W$-mass, the muon $g-2$, and the DM observables in a local $U(1)_{L_\mu - L_\tau}$ model in which a singlet vector-like lepton, a doublet vector-like lepton and a complex singlet $X$ field are introduced in addition to the $U(1)_{L_\mu - L_\tau}$ gauge boson $Z'$ [80] and a complex singlet $\mathcal{S}$ breaking $U(1)_{L_\mu - L_\tau}$ symmetry. As the lightest component of $X$, $X_I$ is a candidate of dark matter (DM) and its heavy partner is $X_R$. The gauge boson self-energy diagrams exchanging the vector-like leptons in the loop can give additional contributions to the oblique parameters ($S,\ T,\ U$), and explain the CDF $W$-mass [24,53,55,76–79]. The interactions between the vector-like leptons and muon mediated by the $X_I$ ($X_R$) can enhance the muon $g-2$ [81–92]. These new particles can affect the DM relic density via the DM pair-annihilation and various co-annihilations processes.

Our work is organized as follows. In Sect. 2 we introduce the model. In Sects. 3 and 4 we study the W-boson mass, muon g-2 anomaly, and the DM observables imposing relevant theoretical and experimental constraints. Finally, we give our conclusion in Sect. 5.

## 2 The model

In addition to the $U(1)_{L_\mu - L_\tau}$ gauge boson $Z'$, we introduce a complex singlet $\mathcal{S}$ breaking $U(1)_{L_\mu - L_\tau}$, a complex singlet

[a] e-mail: leiwang@ytu.edu.cn (corresponding author)

$X$, and the following vector-like lepton fields,

$$E''_{L,R} = \begin{pmatrix} N_{L,R} \\ e''_{L,R} \end{pmatrix}, \; E'_{L,R}. \tag{3}$$

Their quantum numbers under the gauge group $SU(3)_C \times SU(2)_L \times U(1)_Y \times U(1)_{L_\mu - L_\tau}$ are displayed in Table 1, and the $q_x$ is the $U(1)_{L_\mu - L_\tau}$ charge of the $X$ field.

The new Lagrangian respecting the $SU(3)_C \times SU(2)_L \times U(1)_Y \times U(1)_{L_\mu - L_\tau}$ symmetry is written as

$$\begin{aligned} \mathcal{L} = &-\frac{1}{4} Z'_{\mu\nu} Z'^{\mu\nu} + g_{Z'} Z'^{\mu} (\bar{\mu}\gamma_\mu \mu + \bar{\nu}_{\mu_L}\gamma_\mu \nu_{\mu_L} \\ &- \bar{\tau}\gamma_\mu \tau - \bar{\nu}_{\tau_L}\gamma_\mu \nu_{\tau_L}) \\ &+ \bar{E}''(i \not{D}) E'' + \bar{E}'(i \not{D}) E' + (D_\mu X^\dagger)(D^\mu X) \\ &+ (D_\mu \mathcal{S}^\dagger)(D^\mu \mathcal{S}) - V + \mathcal{L}_{\rm Y}, \end{aligned} \tag{4}$$

where $\mu$ and $\tau$ denote the SM muon and tau leptons, and $\nu_\mu$ and $\nu_\tau$ are the corresponding neutrinos. The $D_\mu$ is the covariant derivative and $g_{Z'}$ is the gauge coupling constant of the $U(1)_{L_\mu - L_\tau}$ group. The kinetic mixing term of gauge bosons of $U(1)_{L_\mu - L_\tau}$ and $U(1)_Y$ is severely constrained from the electroweak precision data [93], and therefore we ignore it simply in this paper. The field strength tensor $Z'_{\mu\nu} = \partial_\mu Z'_\nu - \partial_\nu Z'_\mu$, and $V$ and $\mathcal{L}_{\rm Y}$ indicate the scalar potential and Yukawa interactions.

The scalar potential $V$ is written as

$$\begin{aligned} V = &-\mu_h^2 (H^\dagger H) - \mu_S^2 (\mathcal{S}^\dagger \mathcal{S}) + m_X^2 (X^\dagger X) \\ &+ \left[\mu X^2 \mathcal{S} + \text{h.c.}\right] + \lambda_H (H^\dagger H)^2 + \lambda_S (\mathcal{S}^\dagger \mathcal{S})^2 \\ &+ \lambda_X (X^\dagger X)^2 + \lambda_{SX} (\mathcal{S}^\dagger \mathcal{S})(X^\dagger X) + \lambda_{HS} (H^\dagger H)(\mathcal{S}^\dagger \mathcal{S}) \\ &+ \lambda_{HX} (H^\dagger H)(X^\dagger X), \end{aligned} \tag{5}$$

where the SM Higgs doublet $H$, the complex singlet fields $\mathcal{S}$ and $X$ are

$$\begin{aligned} H &= \begin{pmatrix} G^+ \\ \frac{1}{\sqrt{2}} (h_1 + v_h + iG) \end{pmatrix}, \quad \mathcal{S} = \frac{1}{\sqrt{2}} (h_2 + v_S + i\omega), \\ X &= \frac{1}{\sqrt{2}} (X_R + i X_I). \end{aligned} \tag{6}$$

Here $H$ and $\mathcal{S}$ respectively acquire vacuum expectation values (VEVs), $v_h = 246$ GeV and $v_S$, and the VEV of $X$ field is zero. The parameters $\mu_h^2$ and $\mu_S^2$ are determined by the minimization conditions for Higgs potential,

$$\begin{aligned} \mu_h^2 &= \lambda_H v_h^2 + \frac{1}{2}\lambda_{HS} v_S^2, \\ \mu_S^2 &= \lambda_S v_S^2 + \frac{1}{2}\lambda_{HS} v_h^2. \end{aligned} \tag{7}$$

The complex scalar $X$ is split into two real scalar fields $X_R$ and $X_I$ by the $\mu$ term after the $\mathcal{S}$ field acquires VEV $v_S$. Their masses are

$$\begin{aligned} m_{X_R}^2 &= m_X^2 + \frac{1}{2}\lambda_{HX} v_H^2 + \frac{1}{2}\lambda_{SX} v_S^2 + \sqrt{2}\mu v_S \\ m_{X_I}^2 &= m_X^2 + \frac{1}{2}\lambda_{HX} v_H^2 + \frac{1}{2}\lambda_{SX} v_S^2 - \sqrt{2}\mu v_S. \end{aligned} \tag{8}$$

Because the $X$ field has no VEV, there is a remnant discrete $Z_2$ symmetry which makes the lightest component $X_I$ to be stable and as a candidate of DM.

The $\lambda_{HS}$ term leads to a mixing of $h_1$ and $h_2$, and their mass eigenstates $h$ and $S$ are obtained from following relation,

$$\begin{pmatrix} h_1 \\ h_2 \end{pmatrix} = \begin{pmatrix} \cos\alpha & \sin\alpha \\ -\sin\alpha & \cos\alpha \end{pmatrix} \begin{pmatrix} h \\ S \end{pmatrix} \tag{9}$$

with $\alpha$ being the mixing angle. From the $\lambda_{HS}$ term and $\lambda_{HX}$ term, we can obtain the 125 GeV Higgs $h$ coupling to a pair of DM. In order to escape the strong bounds of the DM indirect detection and direct detection experiments, we simply assume the $hX_IX_I$ coupling to be absent, namely choosing $\lambda_{HS} = 0$ and $\lambda_{HX} = 0$. Thus we obtain

$$\alpha = 0, \quad \lambda_H = \frac{m_h^2}{2v_h^2}, \quad \lambda_S = \frac{m_S^2}{2v_S^2}. \tag{10}$$

The gauge boson $Z'$ acquires a mass after $\mathcal{S}$ breaks the $U(1)_{L_\mu - L_\tau}$ symmetry,

$$m_{Z'} = 2g_{Z'} \mid q_x \mid v_S. \tag{11}$$

The Yukawa interactions with the $U(1)_{L_\mu - L_\tau}$ symmetry are given as

$$\begin{aligned} &-\mathcal{L}_{\rm Y,mass} \\ &= m_1 \overline{E'_L} E'_R + m_2 \overline{E''_L} E''_R + \kappa_1 \overline{\mu_R} X E'_L + \kappa_2 \overline{L_\mu} X E''_R \\ &\quad + \sqrt{2} y_1 \overline{E''_L} H E'_R + \sqrt{2} y_2 \overline{E''_R} H E'_L \\ &\quad + \frac{\sqrt{2} m_\mu}{v} \overline{L_\mu} H \mu_R + \text{h.c.}, \end{aligned} \tag{12}$$

where $L_\mu = (\nu_{\mu L}, \mu_L)$.

Since the $X$ field has no VEV, there is no mixing between the vector-like leptons and the muon lepton. However, there is a mixing between the vector-like leptons $E''$ and $E'$ after the $H$ acquires the VEV, $v_h = 246$ GeV, and their mass matrix is given as

$$M_E = \begin{pmatrix} m_1 & y_2 v_h \\ y_1 v_h & m_2 \end{pmatrix}. \tag{13}$$

We take two unitary matrices to diagonalize the mass matrix,

$$U_L = \begin{pmatrix} c_L & -s_L \\ s_L & c_L \end{pmatrix}, \quad U_R = \begin{pmatrix} c_R & -s_R \\ s_R & c_R \end{pmatrix},$$

**Table 1** The quantum numbers of the fields charged under $U(1)_{L_\mu - L_\tau}$. The charge of the other field is zero

| | $SU(3)_c$ | $SU(2)_L$ | $U(1)_Y$ | $U(1)_{L_\mu - L_\tau}$ |
|---|---|---|---|---|
| $E''_{L,R}$ | **1** | **2** | $-1/2$ | $1-q_x$ |
| $E'_{L,R}$ | **1** | **1** | $-1$ | $1-q_x$ |
| $X$ | **1** | **1** | 0 | $q_x$ |
| $\mathcal{S}$ | **1** | **1** | 0 | $-2q_x$ |
| $L_\mu$ | **1** | **2** | $-1/2$ | 1 |
| $\mu_R$ | **1** | **1** | $-1$ | 1 |
| $L_\tau$ | **1** | **2** | $-1/2$ | $-1$ |
| $\tau_R$ | **1** | **1** | $-1$ | $-1$ |

"1" and "2" denote the singlet and the doublet, respectively

$$U_L^\dagger M_E U_R = \text{diag}\left(m_{E_1}, m_{E_2}\right), \tag{14}$$

where $c^2_{L,R} + s^2_{L,R} = 1$. The $E_1$ and $E_2$ are the mass eigenstates of charged vector-like leptons, and the mass of neutral vector-like lepton $N$ is

$$m_N = m_2 = m_{E_2} c_L c_R + m_{E_1} s_L s_R. \tag{15}$$

From the Eq. (12), we can obtain the interactions between the charged vector-like leptons and muon mediated by $X_R$ and $X_I$,

$$-\mathcal{L}_X \supset \frac{1}{\sqrt{2}}(X_R + iX_I)\,[\bar{\mu}_R(\kappa_1 c_L E_{1L} - \kappa_1 s_L E_{2L}) + \bar{\mu}_L(\kappa_2 s_R E_{1R} + \kappa_2 c_R E_{2R})] + h.c., \tag{16}$$

and the 125 GeV Higgs interactions to the charged vector-like leptons $E_1$ and $E_2$,

$$-\mathcal{L}_h \supset \frac{m_{E_1}(c_L^2 s_R^2 + c_R^2 s_L^2) - 2m_{E_2} s_L c_L s_R c_R}{v_h}\, h\bar{E}_1 E_1, + \frac{m_{E_2}(s_L^2 c_R^2 + c_L^2 s_R^2) - 2m_{E_1} s_L c_L s_R c_R}{v_h}\, h\bar{E}_2 E_2. \tag{17}$$

## 3 The $S, T, U$ parameters, $W$-mass, and muon $g-2$

In addition to $m_h = 125$ GeV, $v_h = 246$ GeV, $\lambda_{HS} = 0$, $\lambda_{HX} = 0$, there are many new parameters in the model. We take $g_{Z'}$, $q_x$, $m_{Z'}$, $\lambda_X$, $\lambda_{SX}$, $m_S$, $m_{X_R}$, $m_{X_I}$, $m_{E_1}$, $m_{E_2}$, $s_L$, $s_R$, $\kappa_1$, and $\kappa_2$ as the input parameters, which can be used to determine other parameters.

In order to maintain the perturbativity, we conservatively take

$$|\lambda_{SX}| \leq 4\pi, \quad |\lambda_X| \leq 4\pi, \quad -1 \leq \kappa_1 \leq 1, \quad -1 \leq \kappa_2 \leq 1. \tag{18}$$

The mixing parameters $s_L$ and $s_R$ are taken as

$$-\frac{1}{\sqrt{2}} \leq s_L \leq \frac{1}{\sqrt{2}}, \quad -\frac{1}{\sqrt{2}} \leq s_R \leq \frac{1}{\sqrt{2}}. \tag{19}$$

We take the random uniform sampling method to scan over the input mass parameters in the following ranges:

$$60\text{ GeV} \leq m_{X_I} \leq 500\text{ GeV}, \quad m_{X_I} \leq m_{X_R} \leq 1\text{ TeV}, \quad m_{X_I} \leq m_{E_1} \leq 1\text{ TeV}, \quad m_{X_I} \leq m_{E_2} \leq 1\text{ TeV}, \quad 100\text{ GeV} \leq m_{Z'} \leq 1\text{TeV}, \quad 100\text{ GeV} \leq m_S \leq 1\text{ TeV}. \tag{20}$$

The mass of neutral vector-like lepton $N$ is determined by $m_{E_1}, m_{E_2}, s_L$ and $s_R$, we require $m_N > m_{X_I}$. We choose $0 < g_{Z'}/m_{Z'} \leq (550\text{ GeV})^{-1}$ to satisfy the bound of the neutrino trident process [94]. We take $-2 < q_x \leq 2$, and require $|g_{Z'}(1-q_x)| \leq 1$ and $g_{Z'} \leq 1$ to respect the perturbativity of the $Z'$ couplings.

The tree-level stability of the potential in Eq. (5) impose the following bounds,

$$\lambda_H \geq 0, \quad \lambda_S \geq 0, \quad \lambda_X \geq 0, \quad \lambda_{HS} \geq -2\sqrt{\lambda_H \lambda_S}, \quad \lambda_{HX} \geq -2\sqrt{\lambda_H \lambda_X}, \quad \lambda_{SX} \geq -2\sqrt{\lambda_S \lambda_X}, \quad \sqrt{\lambda_{HS} + 2\sqrt{\lambda_H \lambda_S}}\sqrt{\lambda_{HX} + 2\sqrt{\lambda_H \lambda_X}}\sqrt{\lambda_{SX} + 2\sqrt{\lambda_S \lambda_X}} + 2\sqrt{\lambda_H \lambda_S \lambda_X} + \lambda_{HS}\sqrt{\lambda_X} + \lambda_{HX}\sqrt{\lambda_S} + \lambda_{SX}\sqrt{\lambda_H} \geq 0. \tag{21}$$

The $H \to \gamma\gamma$ decay can be corrected by the loops of the charged vector-like leptons $E_1$ and $E_2$. We impose the bound of the diphoton signal strength of the 125 GeV Higgs [95],

$$\mu_{\gamma\gamma} = 1.10 \pm 0.07. \tag{22}$$

### 3.1 The $S, T, U$ parameters and $W$-mass

The model contains the interactions of gauge bosons and vector-like leptons,

$$-\mathcal{L}_{VG} = -e\gamma \bar{E}_{1,2}\gamma^\mu E_{1,2} + Z\bar{E}_i \gamma^\mu (L_{ij} P_L + R_{ij} P_R) E_j + \frac{g}{2c_W} Z\bar{N}\gamma^\mu (P_L + P_R) N$$

$$+\frac{1}{\sqrt{2}}W^+\bar{N}\gamma^\mu[(c_L P_L + c_R P_R)E_2 + (s_L P_L + s_R P_R)E_1] + h.c., \quad (23)$$

where $L_{ij}$ and $R_{ij}$ are

$$L(R)_{11} = A_1 c^2_{L(R)} + A_2 s^2_{L(R)}, \quad L(R)_{22} = A_1 s^2_{L(R)} + A_2 c^2_{L(R)},$$
$$L(R)_{12} = L(R)_{21} = (A_2 - A_1) s_{L(R)} c_{L(R)} \quad (24)$$

with

$$A_1 = \frac{g}{c_W} s_W^2, \quad A_2 = \frac{g}{c_W}\left(-\frac{1}{2} + s_W^2\right), \quad (25)$$

where $s_W \equiv \sin\theta_W$ and $c_W = \sqrt{1 - s_W^2}$, and $\theta_W$ is the weak mixing angle.

The gauge boson self-energy diagrams exchanging the vector-like leptons in the loop can give additional contributions to the oblique parameters $(S,\ T,\ U)$ [96,97], which are calculated as in Refs. [96–99]

$$\alpha(M_Z^2)\,S = \frac{4s_W^2 c_W^2}{M_Z^2}\left[\Pi^{\rm NP}_{ZZ}(M_Z^2) - \Pi^{\rm NP}_{ZZ}(0) - \Pi^{\rm NP}_{\gamma\gamma}(M_Z^2) - \frac{c_W^2 - s_W^2}{c_W s_W}\Pi^{\rm NP}_{\gamma Z}(M_Z^2)\right], \quad (26)$$

$$\alpha(M_Z^2)\,T = \frac{\Pi^{\rm NP}_{WW}(0)}{M_W^2} - \frac{\Pi^{\rm NP}_{ZZ}(0)}{M_Z^2}, \quad (27)$$

$$\alpha(M_Z^2)\,U = 4s_W^2\left[\frac{\Pi^{\rm NP}_{WW}(M_W^2) - \Pi^{\rm NP}_{WW}(0)}{M_W^2} - c_W^2\left(\frac{\Pi^{\rm NP}_{ZZ}(M_Z^2) - \Pi^{\rm NP}_{ZZ}(0)}{M_Z^2}\right) - 2s_W c_W\frac{\Pi^{\rm NP}_{\gamma Z}(M_Z^2)}{M_Z^2} - s_W^2\frac{\Pi^{\rm NP}_{\gamma\gamma}(M_Z^2)}{M_Z^2}\right], \quad (28)$$

where the $\Pi^{\rm NP}$ function is given in Appendix A.

Analyzing precision electroweak data and the new CDF $W$-mass, Ref. [10] gave the values of $S$, $T$ and $U$,

$$S = 0.06 \pm 0.10, \quad T = 0.11 \pm 0.12, \quad U = 0.14 \pm 0.09 \quad (29)$$

with correlation coefficients

$$\rho_{ST} = 0.9, \quad \rho_{SU} = -0.59, \quad \rho_{TU} = -0.85. \quad (30)$$

The $W$-boson mass is given as [97],

$$\Delta m_W^2 = \frac{\alpha c_W^2}{c_W^2 - s_W^2} m_Z^2\left(-\frac{1}{2}S + c_W^2 T + \frac{c_W^2 - s_W^2}{4s_W^2}U\right). \quad (31)$$

We perform a fit to the values of $S$, $T$, $U$, and require $\chi^2 < \chi^2_{\rm min} + 6.18$ with $\chi^2_{\rm min}$ denoting the minimum of $\chi^2$. We find the best fit point at which $\chi^2_{\rm min} = 1.77$ and $m_W = 80.4381$ GeV. These surviving samples mean to be within the $2\sigma$ range in any two-dimension plane of the model parameters fitting to the $S$, $T$, and $U$ parameters.

In Fig. 1, we show the samples explaining the CDF $W$-boson mass within $2\sigma$ range while satisfying the constraints of the oblique parameters and theoretical constraints. Figure 1 shows that the explanation of the CDF $W$-mass requires appropriate mass splittings among $E_1$, $E_2$ and $N$, which do not simultaneously equal to zero. For example, when $m_{E_2} = m_N$, the mass splitting between $m_{E_1}$ and $m_{E_2}(m_N)$ is required to be larger than 100 GeV. The corrections of the model to $m_W$ tend to increase with $\mid m_{E_2} - m_{E_1} \mid$ and $\mid s_L - s_R \mid$. Thus, the measurement of CDF $W$-mass tends to favor a large (small) $\mid m_{E_2} - m_{E_1} \mid$ for a small (large) $\mid s_L - s_R \mid$, which leads to two clearly distinct populations in $\mid m_{E_2} - m_{E_1} \mid$ of the right panel. From Eq. (15) we obtain

$$\mid m_{E_2} - m_N \mid = \mid m_{E_2}(1 - c_L c_R) - m_{E_1} s_L s_R \mid, \quad (32)$$

and $\mid m_{E_2} - m_N \mid < 50$ GeV favors $s_L$ and $s_R$ to be around 0. However, in such small $s_L$ and $s_R$ region, the CDF $W$-boson mass and the oblique parameters disfavor a large $\mid m_{E_2} - m_{E_1} \mid$, as shown in the right panel of Fig. 1. As a result, a gulf-like structure appears in the left panel for $\mid m_{E_2} - m_N \mid < 50$ GeV and $\mid m_{E_2} - m_{E_1} \mid > 400$ GeV. Assuming $s_L = s_R$ simply we can find that $\mid m_{E_2} - m_N \mid$ is proportional to $\mid m_{E_2} - m_{E_1} \mid$ and $s_L s_R$ from Eq. (32). However, when $\mid m_{E_2} - m_{E_1} \mid$ has a very large value, the CDF $W$-boson mass and the oblique parameters favor relative small $s_L$ and $s_R$ (see the right panel). Therefore, $\mid m_{E_2} - m_N \mid$ has a maximal value for a moderate $\mid m_{E_2} - m_{E_1} \mid$. As a result, a peak-like structure appears in the left panel for which $\mid m_{E_2} - m_N \mid$ reaches 250 GeV for $\mid m_{E_2} - m_{E_1} \mid$ around 500 GeV. Also the similar peak-like and gulf-like structures appear in the middle panel since $\mid m_{E_1} - m_N \mid$ can be derived from $\mid m_{E_2} - m_{E_1} \mid$ and $\mid m_{E_2} - m_N \mid$.

The surviving samples in the Fig. 1 are projected on the plane of U and T, see Fig. 2. The authors of Ref. [10] used GFitter [100] to perform a fit to the new CDF $W$-mass and precision electroweak data, and gave the values of $S$, $T$ and $U$ in Eq. (29) [10]. The result of Ref. [10] is independent on model, and the $U$ parameter is pushed to a large value. From Fig. 2, we see that the correction of the model to T is dominant over U and S. Since the values of $S$, $T$ and $U$ in Eq. (29) are correlated, a large T and a small U can give a well fit to the values of $S$, $T$ and $U$ in Eq. (29) and explain the CDF $W$-mass.

Now we discuss the T parameter. The function $\Pi^{\rm NP}_{WW}(0)$ is zero for $m_{E_2} = m_N$ and $m_{E_1} = m_N$, and the $\Pi^{\rm NP}_{ZZ}(0)$ is zero for $m_{E_2} = m_{E_1}$. Therefore, from Eq. (27) we see that the corrections of the model to $T$ parameter are absent for $m_{E_2} = m_{E_1} = m_N$, which is disfavored by the CDF measurement of $W$ mass. Because there is no mixing between $E_2$ and $E_1$ for $s_L = s_R = 0$, both the $ZE_2E_1$ and $WE_1N$ couplings disappear and $m_{E_2}$ equals to $m_N$. Therefore, for

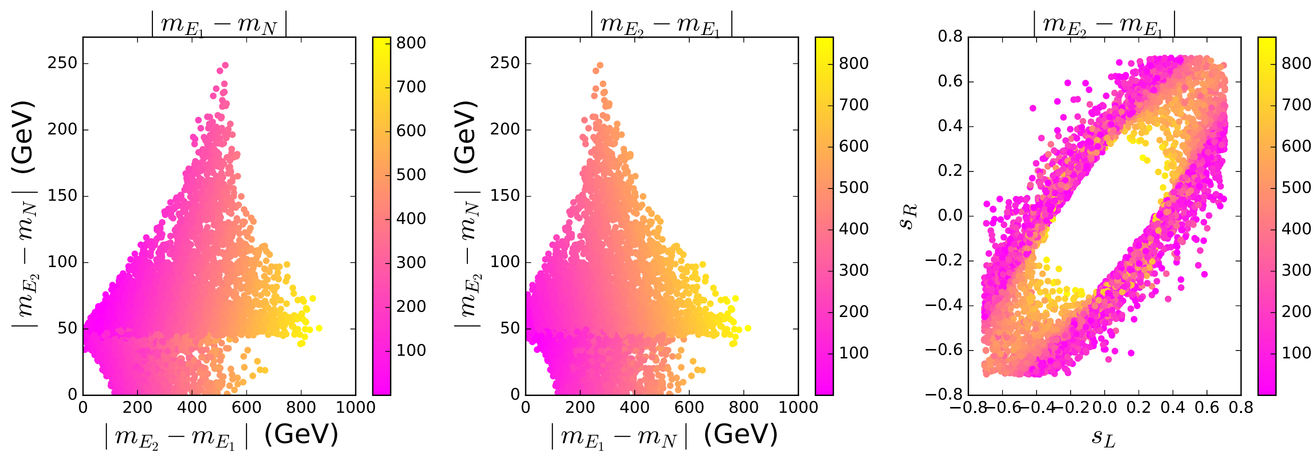


**Fig. 1** The surviving samples explaining the CDF $W$-mass within $2\sigma$ range while satisfying the oblique parameters and theory constraints. The varying colors in each panel indicate the values of $|m_{E_1} - m_N|$ and $|m_{E_2} - m_{E_1}|$, respectively

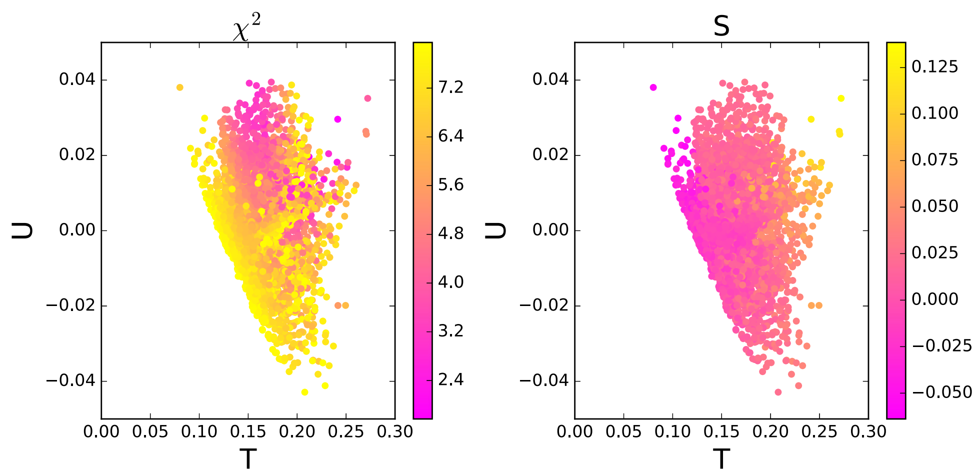


**Fig. 2** Same as Fig. 1, but projected on the plane of U and T. The varying colors in each panel indicate the values of $\chi^2$ and $S$, respectively

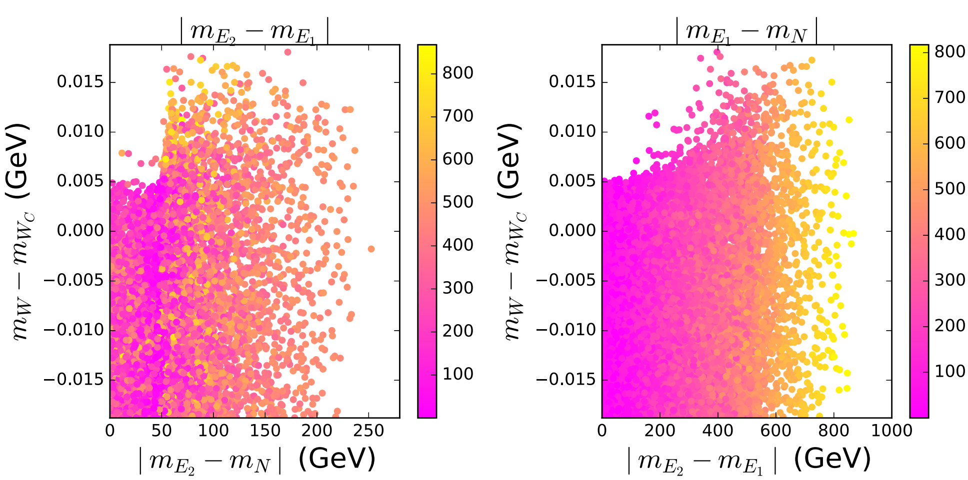


**Fig. 3** Same as Fig. 1, but projected on the planes of $m_W$ versus $|m_{E_2} - m_N|$ and $|m_{E_2} - m_{E_1}|$. Here $m_{W_C}$ denotes the central value of the CDF $W$-mass, 80.4335 GeV. The varying colors in each panel indicate the values of $|m_{E_2} - m_{E_1}|$ and $|m_{E_1} - m_N|$, respectively

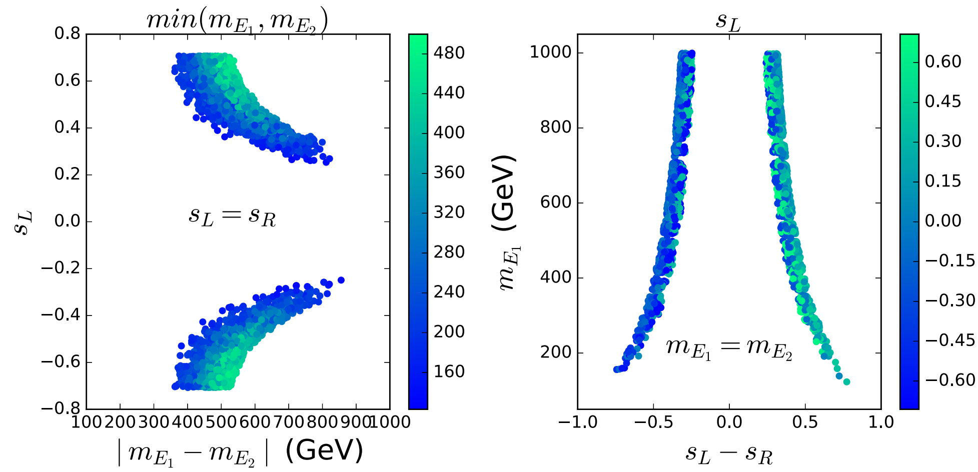


**Fig. 4** All the samples explaining the muon $g-2$ anomaly while satisfying the constraints of "pre $(g-2)_\mu$". The varying colors in each panel indicate the values of $min(m_{E_1}, m_{E_2})$ and $s_L$, and the $min(m_i, m_j, ...)$ denotes the minimal value of $m_i, m_j, ...$

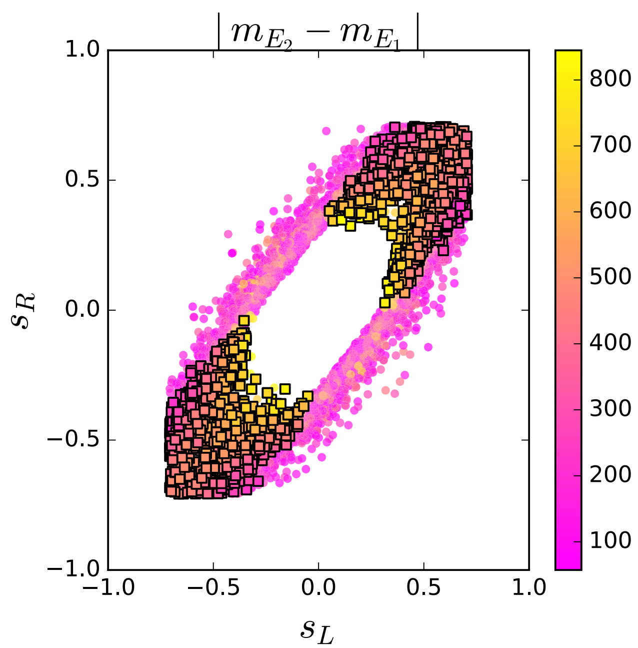


**Fig. 5** All the samples explaining the muon $g-2$ anomaly while satisfying the constraints of "pre $(g-2)_\mu$". The squares and circles are allowed and excluded by the diphoton signal data of 125 GeV Higgs, respectively. The varying colors indicate the values of $|m_{E_2} - m_{E_1}|$

$s_L = s_R = 0$, both $\Pi^{NP}_{WW}(0)$ and $\Pi^{NP}_{ZZ}(0)$ are zero, and the corrections to $T$ parameter are also absent. The case of $s_L = s_R = 0$ is disfavored by the CDF measurement of $W$-mass.

The corrections of the model to $W$-mass are sensitive to the mass differences between the vector-like leptons. In Fig. 3 we show the $W$-mass as a function of $|m_{E_2} - m_N|$ and $|m_{E_2} - m_{E_1}|$.

### 3.2 The muon $g-2$

The model can give additional corrections to the muon $g-2$ via the one-loop diagrams containing the interactions between muon and $E_1$ ($E_2$) mediated by $X_R$ and $X_I$, and the main corrections are calculated as in Refs. [81,83,101]

$$\Delta a_\mu = \frac{1}{32\pi^2} m_\mu \big(\kappa_1 c_L \kappa_2 s_R H(m_{E_1}, m_{X_R}) - \kappa_1 s_L \kappa_2 c_R H(m_{E_2}, m_{X_R}) + \kappa_1 c_L \kappa_2 s_R H(m_{E_1}, m_{X_I}) - \kappa_1 s_L \kappa_2 c_R H(m_{E_2}, m_{X_I})\big), \tag{33}$$

where the function

$$H(m_f, m_\phi) = \frac{m_f}{m_\phi^2} \frac{(r^2 - 4r + 2\log r + 3)}{(r-1)^3} \tag{34}$$

with $r = \frac{m_f^2}{m_\phi^2}$. Also the one-loop diagram containing the interactions of $Z'\mu^+\mu^-$ gives additional correction to the muon $g-2$, which can be safely ignored since the mass of $Z'$ is taken to be $\mathcal{O}(10^2)$ GeV. Equation (33) shows that the correction of the model to the muon $g-2$ is absent for $m_{E_1} = m_{E_2}$ and $s_L = s_R$.

We respectively take $s_L = s_R$ and $m_{E_1} = m_{E_2}$, and show the samples explaining the muon $g-2$ anomaly within $2\sigma$ range while satisfying the constraints "pre $(g-2)_\mu$" (denoting theory constraints, the oblique parameters, and the CDF $W$-mass) in Fig. 4. From Fig. 4, we see that the explanation of the muon $g-2$ anomaly favors $|s_L|$ to decrease with increasing of $|m_{E_1} - m_{E_2}|$ for $s_L = s_R$, and $m_{E_1}$ to increase with decreasing of $|s_L - s_R|$. This characteristic can be well understood from Eq. (33).

After imposing the constraints of the diphoton signal data of the 125 GeV Higgs and "pre $(g-2)_\mu$", we scan over the parameter space, and project the samples explaining the muon $g-2$ anomaly in Fig. 5. We find that the diphoton signal data of the 125 GeV Higgs exclude some samples explaining

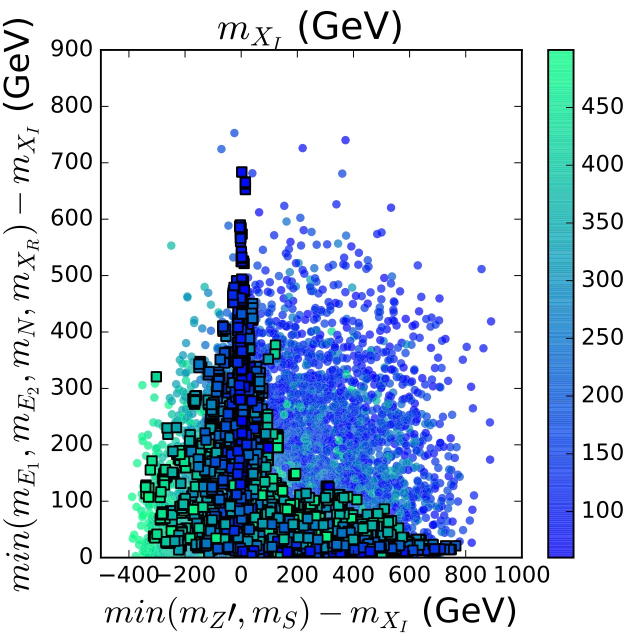


**Fig. 6** All samples satisfy the constraints of "pre $(g-2)_\mu$", the diphoton signal data of the 125 GeV Higgs, and muon $g-2$. The squares and circles are allowed and excluded by the DM relic density respectively. The varying colors indicate the values of $m_{X_I}$

the muon $g-2$ anomaly, and favors $s_L$ and $s_R$ to have same sign, especially for large $\mid s_L \mid$ and $\mid s_R \mid$. When $s_L$ and $s_R$ have same sign, the terms of $h\bar{E}_1 E_1$ ($h\bar{E}_2 E_2$) coupling in Eq. (17) are canceled to some extent, which suppresses the corrections of $E_1$ and $E_2$ to the $h \to \gamma\gamma$ decay. The allowed ranges of $s_L$, $c_L$ and $m_{E_{1,2}}$ will be sizably reduced with the enhancement of measurement precision of the diphoton signal. However, it is challenge to completely exclude the parameter space explaining the muon $g-2$ and $W$-mass via the $h \to \gamma\gamma$ measurement with the currently expected sensitives at the future LHC.

## 4 The DM observables

In the model, in addition to $X_I X_I \to \mu^+\mu^-$, and the DM pair-annihilation processes $X_I X_I \to Z'Z'$, $SS$ will be open for $m_{Z'}$ $(m_S)$ $<$ $m_{X_I}$. When the masses of $E_1$, $E_2$, $N$ and $X_R$ are close to $m_{X_I}$, their various co-annihilation processes will play important roles in the DM relic density. We use FeynRules [102] to generate a model file, and employ micrOMEGAs-5.2.13 [103] to calculate the relic density. The Planck collaboration reported the relic density of cold DM in the universe, $\Omega_c h^2 = 0.1198 \pm 0.0015$ [104].

After imposing the constraints of "pre $(g-2)_\mu$", the diphoton signal data of the 125 GeV Higgs, and the muon $g-2$ anomaly, we project the samples achieving the DM relic density within $2\sigma$ range in Fig. 6. Due to the constraints of muon $g-2$ on the interactions between the vector-like leptons and muon mediated by $X_I$, it is not easy to obtain the correct DM relic density only via the $X_I X_I \to \mu^+\mu^-$ annihilation process, and other processes are needed to accelerate the DM annihilation. As shown in Fig. 6, for $min(m_{Z'}, m_S) < m_{X_I}$, the $X_I X_I \to Z'Z'$ or $SS$ will be open and play a main role in achieving the correct relic density. Then the masses of $X_R$, $E_1$, $E_2$ and $N$ are allowed to have sizable deviation from $m_{X_I}$. When $min(m_{Z'}, m_S)$ is larger than $m_{X_I}$ and the $X_I X_I \to Z'Z'$, $SS$ processes are kinematically forbidden, $min(m_{E_1},\ m_{E_2},\ m_N,\ m_{X_R})$ is required to be close to $m_{X_I}$ so that the correct DM relic density is obtained via their co-annihilation processes.

The $X_I$ has no interactions to the SM quark, and its couplings to the muon lepton and vector-like leptons are constrained by the muon $g-2$ anomaly. Therefore, the model can easily satisfy the bound from the direct detection of DM. At the LHC, the vector-like leptons are mainly produced via electroweak processes,

$$\begin{aligned} &p\ p \to \gamma/Z^* \to E_1\bar{E}_{1,2},\ E_2\bar{E}_{1,2},\ N\bar{N},\\ &p\ p \to W^* \to E_{1,2}\bar{N},\ \bar{E}_{1,2}N, \end{aligned} \tag{35}$$

then the decay modes include

$$E_{1,2} \to \mu X_I,\quad N \to \nu_\mu X_I. \tag{36}$$

If kinematically allowed, the following decay modes will be open,

$$E_{1,2} \to \mu X_R,\ WN,\quad E_{1,2} \to ZE_{2,1},\quad N \to \nu_\mu X_R. \tag{37}$$

The $2\mu + E_T^{miss}$ event searches at the LHC can impose strong constraints on the vector-like leptons and DM. The production processes of $2\mu + E_T^{miss}$ in our model are very similar to the electroweak production of charginos and sleptons decaying into final states with $2\ell + E_T^{miss}$ analyzed by ATLAS with 139 fb$^{-1}$ integrated luminosity data [105]. Therefore, we will use this analysis to constrain our model, which is implemented in the MadAnalysis5 [106–108]. We perform simulations for the samples using `MG5_aMC-3.3.2` [109] with `PYTHIA8` [110] and `Delphes-3.2.0` [111]. We apply MadAnalysis5 to identify the best signal region that is statistically the most significant, and check its $1-\mathrm{CL}_s$ value. Assuming 95% confidence level for the exclusion limit, the model with the given parameter space has been excluded if $1-\mathrm{CL}_s > 0.95$, where $\mathrm{CL}_s$ is determined by the procedure in [112] and implemented in MadAnalysis5.

If the DM relic density is achieved via the co-annihilation processes of vector-like lepton, the mass of vector-like lepton is required to be close to $m_{X_I}$. As a result, the $\mu$ from the vector-like lepton decay is too soft to be distinguished at detector, and the scenario can easily satisfy the constraints of the direct searches at LHC. Here, we employ the ATLAS

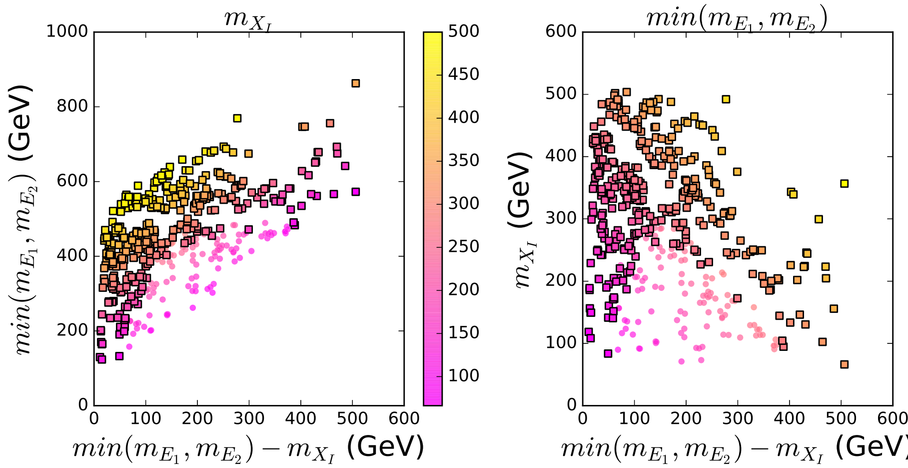


**Fig. 7** For the scenario of $1 < m_{X_R}/m_{X_I} < 1.15$ and $m_{Z'}$ $(m_S) > m_{X_R}$, all samples satisfy the constraints of "pre $(g-2)_\mu$", the diphoton signal data of the 125 GeV Higgs, the muon $g-2$ anomaly, and the DM relic density. The squares and circles are allowed and excluded by the direct searches for $2\ell + E_T^{miss}$ at the LHC. The varying colors in each panel indicate the values of $m_{X_I}$ and $min(m_{E_1}, m_{E_2})$, respectively

analysis of $2\ell + E_T^{miss}$ in Ref. [105] to constrain another scenario in which $1 < m_{X_R}/m_{X_I} < 1.15$ and $m'_Z$ $(m_S) > m_{X_R}$ is taken, and the co-annihilation processes of $X_R$ can play a main role in achieving the correct relic density. Thus, the masses of the vector-like leptons are allowed to be much larger than $m_{X_I}$.

We impose the constraints of "pre $(g-2)_\mu$", the diphoton signal data of the 125 GeV Higgs, the muon $g-2$ anomaly, the DM relic density, and the direct searches for $2\ell + E_T^{miss}$ at the LHC, and project the surviving samples in Fig. 7. From Fig. 7 we see that the mass of the lightest charged vector-like lepton is allowed to be as low as 120 GeV if $min(m_{E_1},\ m_{E_2}) - m_{X_I} < 60$ GeV since the muon becomes soft in the region. As $min(m_{E_1},\ m_{E_2}) - m_{X_I}$ increases, the energy of muon becomes large, and the vector-like lepton needs to be large enough to escape the constraints of direct searches for $2\ell + E_T^{miss}$ at the LHC. For example, $min(m_{E_1},\ m_{E_2})$ is favored to be larger than 500 GeV for $min(m_{E_1},\ m_{E_2}) - m_{X_I} > 300$ GeV. The DM mass is allowed to be as low as 100 GeV if $min(m_{E_1},\ m_{E_2}) - m_{X_I} < 60$ GeV or $min(m_{E_1},\ m_{E_2}) - m_{X_I} > 400$ GeV.

The $p\ p \to E_{1,2}\bar{E}_{1,2} \to \mu^+\mu^- + E_T^{miss}$ is still the most sensitive channel of detecting the vector-like leptons at future LHC. With the enhancement of the integrated luminosity and center-of-mass energy of the LHC, the current surviving parameter space will be furtherly reduced. However, it is challenge to examine the case of the small mass splitting between $min(m_{E_1},\ m_{E_2})$ and $m_{X_I}$ for which the signal contains two soft muon leptons and missing energy. The searches for soft leptons require a dedicated study of the signal and background kinematics beyond a simple cut-and-count analysis. Also the LHC collaborations need design dedicated triggers that have acceptance for leptons with lower transverse momenta. These studies are beyond the scope of this paper.

At the tree-level, the $Z'$ has couplings to the muon lepton, the tau lepton and the new vector-like leptons, and no couplings to the SM quarks. Therefore, for a light $Z'$, the $Z'$ is mainly produced from the decay of $Z$, and then $Z'$ decays into $\mu^+\mu^-$, $\tau^+\tau^-$, $\nu_\mu\bar{\nu}_\mu$, $\nu_\tau\bar{\nu}_\tau$. Thus, the ATLAS and CMS searches for $4\ell$ can impose strong bound on a light $Z'$. Here we take $m_{Z'} > 100$ GeV to avoid the bound of ATLAS and CMS searches for $4\ell$. Also the $Z'$ can be produced in association with a pair of vector-like leptons, and the final states contain the multi-leptons + $E_T^{miss}$. The LHC sensitivities to such processes are much weaker than those of the $2\ell + E_T^{miss}$ discussed above. The scalar $S$ has no couplings to the SM quark, the SM lepton, the SM-like Higgs boson, and the new vector-like leptons at the tree-level. The $S$ can be produced in association with a $Z'$, and the LHC sensitivities are much weaker than those of $Z'$ production processes. Therefore, $m_S > 100$ GeV is a safe choice in this paper.

## 5 Conclusion

In this paper we discussed the CDF $W$-mass, the muon $g-2$, and the DM observables in a local $U(1)_{L_\mu - L_\tau}$ model, and obtained the following observations: (i) The CDF $W$-mass disfavors $m_{E_1} = m_{E_2} = m_N$ or $s_L = s_R = 0$, and favors a large mass splitting between $E_1$ and $E_2$ when the differences between $s_L$ and $s_R$ becomes small. (ii) The muon $g-2$ anomaly can be simultaneously explained for appropriate difference between $s_L$ $(m_{E_1})$ and $s_R$ $(m_{E_2})$, and some regions are excluded by the diphoton signal data of the 125 GeV Higgs. (iii) Combined with the CDF $W$-mass, muon $g-2$ anomaly and other relevant constraints, the correct DM relic density is mainly achieved in two different scenarios: (1) $X_I X_I \to Z'Z'$, $SS$ for $m_{Z'}(m_S) < m_{X_I}$ and (2) the co-annihilation processes for $min(m_{E_1}, m_{E_2}, m_N, m_{X_R})$ close to $m_{X_I}$. (iv) The direct searches for $2\ell + E_T^{miss}$ event at the LHC impose strong bounds on the masses of the vector-like leptons and DM as well as their mass splitting.

**Acknowledgements** We thank Songtao Liu, Shuyuan Guo, Liangliang Shang, Shiyu Wang, and Yang Zhang for the helpful discussions. This work was supported by the National Natural Science Foundation of China under Grant 11975013.

**Data Availability Statement** This manuscript has no associated data or the data will not be deposited. [Authors' comment: The work is purely theoretical, and therefore there is no associated data.]


Funded by SCOAP$^3$. SCOAP$^3$ supports the goals of the International Year of Basic Sciences for Sustainable Development.

## Appendix A: The Π function

The $\Pi_{XY}(p^2, m_1^2, m_2^2)$ and $\Pi_{XY}(0, m_1^2, m_2^2)$ are given as [98, 99]

$$\begin{aligned}
&\Pi_{XY}(p^2, m_1^2, m_2^2) \\
&= -\frac{N_c}{16\pi^2}\left\{\frac{2}{3}\left(g_{LX}^{f_1 f_2} g_{LY}^{f_1 f_2} + g_{RX}^{f_1 f_2} g_{RY}^{f_1 f_2}\right)\right. \\
&\times \left[m_1^2 + m_2^2 - \frac{p^2}{3} - \left(A_0(m_1^2) + A_0(m_2^2)\right)\right. \\
&+ \frac{m_1^2 - m_2^2}{2p^2}\left(A_0(m_1^2) - A_0(m_2^2)\right) \\
&\left.+ \frac{2p^4 - p^2(m_1^2 + m_2^2) - (m_1^2 - m_2^2)^2}{2p^2} B_0(p^2, m_1^2, m_2^2)\right] \\
&\left.+ 2m_1 m_2\left(g_{LX}^{f_1 f_2} g_{RY}^{f_1 f_2} + g_{RX}^{f_1 f_2} g_{LY}^{f_1 f_2}\right) B_0(p^2, m_1^2, m_2^2)\right\},
\end{aligned} \tag{A1}$$

$$\begin{aligned}
&\Pi_{XY}(0, m_1^2, m_2^2) = -\frac{N_c}{16\pi^2}\left\{\frac{2}{3}\left(g_{LX}^{f_1 f_2} g_{LY}^{f_1 f_2} + g_{RX}^{f_1 f_2} g_{RY}^{f_1 f_2}\right)\right. \\
&\times \left[m_1^2 + m_2^2 - \left(A_0(m_1^2) + A_0(m_2^2)\right)\right. \\
&\left.- \frac{m_1^2 + m_2^2}{2} B_0(0, m_1^2, m_2^2) - \frac{(m_1^2 - m_2^2)^2}{2} B_0^{'}(0, m_1^2, m_2^2)\right] \\
&\left.+ 2m_1 m_2\left(g_{LX}^{f_1 f_2} g_{RY}^{f_1 f_2} + g_{RX}^{f_1 f_2} g_{LY}^{f_1 f_2}\right) B_0(0, m_1^2, m_2^2)\right\}.
\end{aligned} \tag{A2}$$

Here the coupling constants $g_{LX}^{f_1 f_2}$ and $g_{RX}^{f_1 f_2}$ are from

$$\overline{f}_1\left(g_{LX}^{f_1 f_2} P_L + g_{RX}^{f_1 f_2} P_R\right)\gamma_\mu f_2 X^\mu, \tag{A3}$$

and the $A_0$, $B_0$, and $B_0^{'}$ functions are

$$\begin{aligned}
A_0(m^2) &= \left(\frac{4\pi\mu^2}{m^2}\right)^\epsilon \Gamma(1+\epsilon)\left(\frac{1}{\epsilon} + 1\right) m^2, \\
B_0(p^2, m_1^2, m_2^2) &= \left(\frac{4\pi\mu^2}{m_2^2}\right)^\epsilon \Gamma(1+\epsilon) \\
&\quad \times \left[\frac{1}{\epsilon} - f_1(p^2, m_1^2, m_2^2)\right], \\
B_0^{'}(p^2, m_1^2, m_2^2) &= \frac{\partial}{\partial p^2} B_0(p^2, m_1^2, m_2^2),
\end{aligned} \tag{A4}$$

and

$$\begin{aligned}
&f_1(p^2, m_1^2, m_2^2) \\
&= \int_0^1 dx \log\left(x + \frac{m_1^2(1-x) - p^2 x(1-x)}{m_2^2}\right).
\end{aligned} \tag{A5}$$

## References

1. CDF Collaboration, High-precision measurement of the W boson mass with the CDF II detector. Science **376**, 6589 (2022)
2. P.A. Zyla et al. (Particle Data Group), Review of particle physics. PTEP **2020**, 083C01 (2020)
3. ATLAS Collaboration, M. Aaboud et al., Measurement of the W-boson mass in pp collisions at $\sqrt{s} = 7$ TeV with the ATLAS detector. Eur. Phys. J. C **78**, 110 (2018)
4. B. Abi et al. (Fermilab Collaboration), Measurement of the positive muon anomalous magnetic moment to 0.46 ppm. Phys. Rev. Lett. **126**, 141801 (2021)
5. Muon g-2 Collaboration, Precise measurement of the positive muon anomalous magnetic moment. Phys. Rev. Lett. **86**, 2227 (2001)
6. Muon g-2 Collaboration, Final report of the muon E821 anomalous magnetic moment measurement at BNL. Phys. Rev. D **73**, 072003 (2006)
7. T. Aoyama, N. Asmussen, M. Benayoun, J. Bijnens, T. Blum, The anomalous magnetic moment of the muon in the Standard Model. Phys. Rep. **887**, 1–166 (2020)
8. T. Blum, N. Christ, M. Hayakawa, T. Izubuchi, L. Jin, C. Jung, C. Lehner, Hadronic light-by-light scattering contribution to the muon anomalous magnetic moment from lattice QCD. Phys. Rev. Lett. **124**, 132002 (2020)
9. G. Colangelo, F. Hagelstein, M. Hoferichter, L. Laub, P. Stoffer, Longitudinal short-distance constraints for the hadronic light-by-light contribution to $(g-2)_\mu$ with large-$N_c$ Regge models. JHEP **03**, 101 (2020)
10. C.-T. Lu, L. Wu, Y. Wu, B. Zhu, Electroweak precision fit and new physics in light of the W boson mass. Phy. Rev. D **106**, 035034 (2022). arXiv:2204.03796
11. Y.-Z. Fan, T.-P. Tang, Y.-L.S. Tsai, L. Wu, Inert Higgs dark matter for new CDF W-boson mass and detection prospects. Phy. Rev. L **129**, 091802 (2022). arXiv:2204.03693
12. P. Athron, A. Fowlie, C.-T. Lu, L. Wu, Y. Wu, B. Zhu, The $W$ boson mass and muon $g-2$: hadronic uncertainties or new physics? arXiv:2204.03996
13. G.-W. Yuan, L. Zu, L. Feng, Y.-F. Cai, Hint on new physics from the $W$-boson mass excess—axion-like particle, dark photon or Chameleon dark energy. arXiv:2204.04183
14. A. Strumia, Interpreting electroweak precision data including the $W$-mass CDF anomaly. JHEP **08**, 248 (2022). arXiv:2204.04191

15. J.M. Yang, Y. Zhang, Low energy SUSY confronted with new measurements of W-boson mass and muon g-2. Sci. Bul. **16**,1430–1436 (2022). arXiv:2204.04202
16. J. d. Blas, M. Pierini, L. Reina, L. Silvestrini, Impact of the recent measurements of the top-quark and W-boson masses on electroweak precision fits. arXiv:2204.04204
17. X. Du, Z. Li, F. Wang, Y.K. Zhang, Explaining the muon $g-2$ anomaly and new CDF II W-boson mass in the framework of (extra)ordinary gauge mediation. arXiv:2204.04286
18. T.-P. Tang, M. Abdughani, L. Feng, Y.-L.S. Tsai, Y.-Z. Fan, NMSSM neutralino dark matter for $W$-boson mass and muon $g-2$ and the promising prospect of direct detection. Phys. Lett. B **832**, 137232 (2022). arXiv:2204.04356
19. G. Cacciapaglia, F. Sannino, The W boson mass weighs in on the non-standard Higgs. Phys. Lett. B **832**, 137232 (2022). arXiv:2204.04514
20. M. Blennow, P. Coloma, E. Fernandez-Martinez, M. Gonzalez-Lopez, Right-handed neutrinos and the CDF II anomaly. Phys. Rev. D **106**, 073005 (2022). arXiv:2204.04559
21. K. Sakurai, F. Takahashi, W. Yin, Singlet extensions and W boson mass in the light of the CDF II result. Phys. Lett. B **833**, 137324 (2022). arXiv:2204.04770
22. J.J. Fan, L. Li, T. Liu, K.-F. Lyu, $W$-boson mass, electroweak precision tests and SMEFT. Phys. Rev. D **106**, 073010 (2022). arXiv:2204.04805
23. X. Liu, S.-Y. Guo, B. Zhu, Y. Li, Unifying gravitational waves with $W$ boson, FIMP dark matter, and Majorana Seesaw mechanism. Sci. Bull. **67**, 1437–1442 (2022). arXiv:2204.04834
24. H.M. Lee, K. Yamashita, A model of vector-like leptons for the muon $g-2$ and the $W$ boson mass. Eur. Phys. J. C **82**, 661 (2022). arXiv:2204.05024
25. Y. Cheng, X.-G. He, Z.-L. Huang, M.-W. Li, Type-II seesaw triplet scalar effects on neutrino trident scattering. Phys. Lett. B **831**, 137218 (2022). arXiv:2204.05031
26. H. Song, W. Su, M. Zhang, Electroweak phase transition in 2HDM under Higgs, Z-pole, and W precision measurements. JHEP **10**, 048 (2022). arXiv:2204.05085
27. E. Bagnaschi, J. Ellis, M. Madigan, K. Mimasu, V. Sanz, T. You, SMEFT analysis of $m_W$. JHEP **08**, 308 (2022). arXiv:2204.05260
28. A. Paul, M. Valli, Violation of custodial symmetry from W-boson mass measurements. Phys. Rev. D **106**, 013008 (2022). arXiv:2204.05267
29. H. Bahl, J. Braathen, G. Weiglein, New physics effects on the $W$-boson mass from a doublet extension of the SM Higgs sector. Phys. Lett. B **833**, 137295 (2022). arXiv:2204.05269
30. P. Asadi, C. Cesarotti, K. Fraser, S. Homiller, A. Parikh, Oblique lessons from the $W$ mass measurement at CDF II. arXiv:2204.05283
31. L.D. Luzio, R. Grober, P. Paradisi, Higgs physics confronts the $M_W$ anomaly. Phys. Lett. B **832**, 137250 (2022). arXiv:2204.05284
32. P. Athron, M. Bach, D.H.J. Jacob, W. Kotlarski, D. Stockinger, A. Voigt, Precise calculation of the W boson pole mass beyond the Standard Model with FlexibleSUSY. Phys. Rev. D **106**, 095023 (2022). arXiv:2204.05285
33. J. Gu, Z. Liu, T. Ma, J. Shu, Speculations on the W-mass measurement at CDF. Chin. Phys. C **46**, 123107 (2022). arXiv:2204.05296
34. J.J. Heckman, Extra $W$-boson mass from a D3-brane. Phys. Lett. B **833**, 137387 (2022). arXiv:2204.05302
35. K.S. Babu, S. Jana, P.K. Vishnu, Correlating $W$-boson mass shift with muon $g-2$ in the 2HDM. arXiv:2204.05303
36. B.-Y. Zhu, S. Li, J.-G. Cheng, R.-L. Li, Y.-F. Liang, Using gamma-ray observation of dwarf spheroidal galaxy to test a dark matter model that can interpret the W-boson mass anomaly. arXiv:2204.04688
37. Y. Heo, D.-W. Jung, J.S. Lee, Impact of the CDF $W$-mass anomaly on two Higgs doublet model. Phys. Lett. B **833**, 137274 (2022). arXiv:2204.05728
38. X.K. Du, Z. Li, F. Wang, Y.K. Zhang, Explaining the new CDF II W-boson mass data in the Georgi–Machacek extension models. arXiv:2204.05760
39. K. Cheung, W.-Y. Keung, P.-Y. Tseng, Isodoublet vector leptoquark solution to the muon g-2, RK,K*, RD,D*, and W-mass anomalies. arXiv:2204.05942
40. A. Crivellin, M. Kirk, T. Kitahara, F. Mescia, Correlating $t \to cZ$ to the $W$ mass and $B$ physics with vector-like quarks. arXiv:2204.05962
41. M. Endo, S. Mishima, New physics interpretation of $W$-boson mass anomaly. Phys. Rev. D **106**, 115005 (2022). arXiv:2204.05965
42. T. Biekotter, S. Heinemeyer, G. Weiglein, Excesses in the low-mass Higgs-boson search and the $W$-boson mass measurement. arXiv:2204.05975
43. R. Balkin, E. Madge, T. Menzo, G. Perez, Y. Soreq, J. Zupan, On the implications of positive W mass shift. JHEP **05**, 133 (2022). arXiv:2204.05992
44. N.V. Krasnikov, Nonlocal generalization of the SM as an explanation of recent CDF result. arXiv:2204.06327
45. Y.H. Ahn, S.K. Kang, R. Ramos, Implications of new CDF-II $W$ boson mass on two Higgs doublet model. Phys. Rev. D **106**, 055038 (2022). arXiv:2204.06485
46. X.-F. Han, F. Wang, L. Wang, J.M. Yang, Y. Zhang, Joint explanation of W-mass and muon g-2 in the 2HDM*. Chin. Phys. C **46**, 103105 (2022)
47. M.-D. Zheng, F.-Z. Chen, H.-H. Zhang, The $W\ell\nu$-vertex corrections to W-boson mass in the R-parity violating MSSM. arXiv:2204.06541
48. P.F. Perez, H.H. Patel, A.D. Plascencia, On the $W$-mass and new Higgs bosons. Phys. Lett. B **833**, 137371 (2022). arXiv:2204.07144
49. S. Kanemura, K. Yagyu, Implication of the W boson mass anomaly at CDF II in the Higgs triplet model with a mass difference. Phys. Lett. B **831**, 137217 (2022). arXiv:2204.07511
50. E. Almeida, A. Alves, O. Eboli, M.C. Gonzalez-Garcia, Impact of CDF-II measurement of $M_W$ on the electroweak legacy of the LHC Run II. arXiv:2204.10130
51. A. Addazi, A. Marciano, R. Pasechnik, H. Yang, CDF II $W$-mass anomaly faces first-order electroweak phase transition. arXiv:2204.10315
52. T.A. Chowdhury, J. Heeck, S. Saad, A. Thapa, $W$ boson mass shift and muon magnetic moment in the Zee model. Phys. Rev. D **106**, 035004 (2022). arXiv:2204.08390
53. J. Kawamura, S. Okawa, Y. Omura, $W$ boson mass and muon $g-2$ in a lepton portal dark matter model. Phys. Rev. D **106**, 015005 (2022). arXiv:2204.07022
54. A. Ghoshal, N. Okada, S. Okada, D. Raut, Q. Shafi, A. Thapa, Type III seesaw with R-parity violation in light of $m_W$ (CDF). arXiv:2204.07138
55. K.I. Nagao, T. Nomura, H. Okada, A model explaining the new CDF II W boson mass linking to muon $g-2$ and dark matter. arXiv:2204.07411
56. D. Borah, S. Mahapatra, D. Nanda, N. Sahu, Type II Dirac seesaw with observable $\Delta N_{eff}$ in the light of W-mass anomaly. Phys. Lett. B **833**, 137297 (2022). arXiv:2204.08266
57. K.-Y. Zhang, W.-Z. Feng, Explaining $W$ boson mass anomaly and dark matter with a $U(1)$ dark sector. arXiv:2204.08067
58. L.M. Carpenter, T. Murphy, M.J. Smylie, Changing patterns in electroweak precision with new color-charged states: oblique corrections and the $W$ boson mass. arXiv:2204.08546
59. O. Popov, R. Srivastava, The triplet Dirac seesaw in the view of the recent CDF-II W mass anomaly. arXiv:2204.08568

60. K. Ghorbani, P. Ghorbani, $W$-boson mass anomaly from scale invariant 2HDM. Nucl. Phys. B **984**, 115980 (2022). arXiv:2204.09001
61. M.X. Du, Z.W. Liu, P. Nath, CDF W mass anomaly from a dark sector with a Stueckelberg–Higgs portal. Phys. Lett. B **834**, 137454 (2022). arXiv:2204.09024
62. A. Bhaskar, A.A. Madathil, T. Mandal, S. Mitra, Combined explanation of $W$-mass, muon $g-2$, $R_{K^{(*)}}$ and $R_{D^{(*)}}$ anomalies in a singlet-triplet scalar leptoquark model. arXiv:2204.09031
63. J. Cao, L. Meng, L. Shang, S. Wang, B. Yang, Interpreting the $W$ mass anomaly in the vectorlike quark models. Phys. Rev. D **106**, 055042 (2022). arXiv:2204.09477
64. S. Baek, Implications of CDF $W$-mass and $(g-2)_\mu$ on $U(1)_{L_\mu-L_\tau}$ model. arXiv:2204.09585
65. D. Borah, S. Mahapatra, N. Sahu, Singlet-doublet fermion origin of dark matter, neutrino mass and W-mass anomaly. Phys. Lett. B **831**, 137196 (2022). arXiv:2204.09671
66. S. Lee, K. Cheung, J. Kim, C.-T. Lu, J. Song, Status of the two-Higgs-doublet model in light of the CDF $m_W$ measurement. Phys. Rev. D **106**, 075013 (2022). arXiv:2204.10338
67. J. Heeck, W-boson mass in the triplet seesaw model. Phys. Rev. D **106**, 015004 (2022). arXiv:2204.10274
68. Y. Cheng, X.-G. He, F. Huang, J. Sun, Z.-P. Xing, Dark photon kinetic mixing effects for CDF W mass excess. arXiv:2204.10156
69. C.F. Cai, D.Y. Qiu, Y.-L. Tang, A.-H. Yu, H.-H. Zhang, Corrections to electroweak precision observables from mixings of an exotic vector boson in light of the CDF $W$-mass anomaly. Phys. Rev. D **106**, 095003 (2022). arXiv:2204.11570
70. R. Benbrik, M. Boukidi, B. Manaut, $W$-mass and 96 GeV excess in type-III 2HDM. arXiv:2204.11755
71. T.Y. Yang, S.T. Qian, S. Deng, J. Xiao, L.Y. Gao, A.M. Levin, Q. Li, M. Lu, Z.Y. You, The physics case for a neutrino lepton collider in light of the CDF W mass measurement. arXiv:2204.11871
72. A. Batra, S. K. A, S. Mandal, H. Prajapati, R. Srivastava, CDF-II $W$ boson mass anomaly in the canonical scotogenic neutrino-dark matter model. arXiv:2204.11945
73. H. Abouabid, A. Arhrib, R. Benbrik, M. Krab, M. Ouchemhou, Is the new CDF $M_W$ measurement consistent with the two Higgs doublet model? arXiv:2204.12018
74. H. Gisbert, V. Miralles, J. Ruiz-Vidal, W-boson mass and electric dipole moments from colour-octet scalars. arXiv:2204.12453
75. X.-Q. Li, Z.-J. Xie, Y.-D. Yang, X.-B. Yuan, Correlating the CDF $W$-boson mass shift with the $b \to s\ell^+\ell^-$ anomalies. arXiv:2205.02205
76. J. Kawamura, S. Raby, $W$ mass in a model with vectorlike leptons and $U(1)^{'}$. Phys. Rev. D **106**, 035009 (2022)
77. T.A. Chowdhury, S. Saad, Leptoquark-vectorlike quark model for $m_W$ (CDF), $(g-2)_\mu$, $R_{K^{(*)}}$ anomalies and neutrino mass. arXiv:2205.03917
78. S.-S. Kim, H.M. Lee, A.G. Menkara, K. Yamashita, $SU(2)_D$ lepton portals for the muon $g-2$, $W$-boson mass, and dark matter. Phys. Rev. D **106**, 015008 (2022)
79. S. Arora, M. Kashav, S. Verma, B.C. Chauhan, Muon $(g-2)$ and W-boson mass anomaly in a model based on $Z_4$ symmetry with vector like fermion. arXiv:2207.08580
80. X.G. He, G.C. Joshi, H. Lew, R.R. Volkas, New-$Z^{'}$ phenomenology. Phys. Rev. D **43**, 22–24 (1991)
81. R. Dermisek, A. Raval, Explanation of the muon $g-2$ anomaly with vectorlike leptons and its implications for Higgs decays. Phys. Rev. D **88**, 013017 (2013)
82. A. Falkowski, D.M. Straub, A. Vicente, Vector-like leptons: Higgs decays and collider phenomenology. JHEP **05**, 092 (2014)
83. J. Kawamura, S. Raby, A. Trautner, Complete vectorlike fourth family and new U(1)′ for muon anomalies. Phys. Rev. D **100**, 055030 (2019)
84. E.J. Chun, J. Kim, Leptonic precision test of leptophilic two-Higgs-doublet model. JHEP **07**, 110 (2016)
85. M. Lindner, M. Platscher, F.S. Queiroz, A call for new physics: the muon anomalous magnetic moment and lepton flavor violation. Phys. Rep. **731**, 1–82 (2018)
86. A. Cherchiglia, D. Stockinger, H. Stockinger-Kim, The muon g − 2 for low-mass pseudoscalar Higgs in the general 2HDM. Phys. Rev. D **98**, 035001 (2018)
87. B. Barman, D. Borah, L. Mukherjee, S. Nandi, Correlating the anomalous results in $b \to s$ decays with inert Higgs doublet dark matter and the muon $g-2$. Phys. Rev. D **100**, 115010 (2019)
88. A. Crivellin, M. Hoferichter, P. Schmidt-Wellenburg, Combined explanations of $(g-2)_{\mu,e}$ and implications for a large muon EDM. Phys. Rev. D **98**, 113002 (2018)
89. A. Crivellin, M. Hoferichter, Consequences of chirally enhanced explanations of $(g-2)_\mu$ for $h \to \mu\mu$ and $Z \to \mu\mu$. JHEP **07**, 135 (2021)
90. L. Wang, J.M. Yang, M. Zhang, Y. Zhang, Revisiting lepton-specific 2HDM in light of muon $g-2$ anomaly. Phys. Lett. B **788**, 519–529 (2019)
91. A.E.C. Hernandez, S.F. King, H. Lee, Fermion mass hierarchies from vectorlike families with an extended 2HDM and a possible explanation for the electron and muon anomalous magnetic moments. Phys. Rev. D **103**, 115024 (2021)
92. H. Bharadwaj, S. Dutta, A. Goyal, Leptonic g-2 anomaly in an extended Higgs sector with vector-like leptons. JHEP **11**, 056 (2021)
93. A. Hook, E. Izaguirre, J.G. Wacker, Model-independent bounds on kinetic mixing. Adv. High Energy Phys. **2011**, 859762 (2011)
94. W. Altmannshofer, S. Gori, M. Pospelov, I. Yavin, Neutrino trident production: a powerful probe of new physics with neutrino beams. Phys. Rev. Lett. **113**, 091801 (2014)
95. L. Workman et al. (Particle Data Group), Review of particle physics. Prog. Theor. Exp. Phys. **2022**, 083C01 (2022)
96. M.E. Peskin, T. Takeuchi, New constraint on a strongly interacting Higgs sector. Phys. Rev. Lett. **65**, 964 (1990)
97. M.E. Peskin, T. Takeuchi, Estimation of oblique electroweak corrections. Phys. Rev. D **46**, 381–409 (1992)
98. M.-C. Chen, S. Dawson, One-loop radiative corrections to the $\rho$ parameter in the littlest Higgs model. Phys. Rev. D **70**, 015003 (2004)
99. S.K. Garg, C.S. Kim, Vector like leptons with extended Higgs sector. arXiv:1305.4712
100. M. Baak, J. Cúth, J. Haller, A. Hoecker, R. Kogler, K. Monig, M. Schott, J. Stelzer (Gfitter Group), The global electroweak fit at NNLO and prospects for the LHC and ILC. Eur. Phys. J. C **74**, 3046 (2014)
101. F. Jegerlehner, A. Nyffeler, The muon g-2. arXiv:0902.3360
102. A. Alloul et al., FeynRules 2.0—a complete toolbox for tree-level phenomenology. Comput. Phys. Commun. **185**, 2250 (2014)
103. G. Belanger, F. Boudjema, A. Pukhov, A. Semenov, micrOMEGAs_3: a program for calculating dark matter observables. Comput. Phys. Commun. **185**, 960–985 (2014)
104. Planck Collaboration, Planck 2015 results. XXVII. The second Planck catalogue of Sunyaev–Zeldovich sources. Astron. Astrophys. A **27**, 594 (2016)
105. ATLAS Collaboration, Search for electroweak production of charginos and sleptons decaying into final states with two leptons and missing transverse momentum in $\sqrt{s} = 13$ TeV $pp$ collisions using the ATLAS detector. Eur. Phys. J. C **80**, 123 (2020)
106. E. Conte, B. Fuks, Confronting new physics theories to LHC data with MADANALYSIS 5. Int. J. Mod. Phys. A **33**, 1830027 (2018)
107. J.Y. Araz, M. Frank, B. Fuks, Reinterpreting the results of the LHC with MadAnalysis 5: uncertainties and higher-luminosity estimates. Eur. Phys. J. C **80**, 531 (2020)

108. J.Y. Araz, B. Fuks, G. Polykratis, Simplified fast detector simulation in MADANALYSIS 5. Eur. Phys. J. C **81**, 329 (2021)
109. J. Alwall et al., The automated computation of tree-level and next-to-leading order differential cross sections, and their matching to parton shower simulations. JHEP **1407**, 079 (2014)
110. P. Torrielli, S. Frixione, Matching NLO QCD computations with PYTHIA using MCNLO. JHEP **1004**, 110 (2010)
111. J. de Favereau et al. (DELPHES 3 Collaboration), DELPHES 3, a modular framework for fast simulation of a generic collider experiment. JHEP **1402**, 057 (2014)
112. A.L. Read, Presentation of search results: the CLs technique. J. Phys. G **28**, 2693–2704 (2002)